Available online at www.sciencedirect.com
SCIENCE DIRECT®
Bioorganic & Medicinal Chemistry 13 (2005) 5658–5667
Bioorganic & Medicinal Chemistry

Density-functional theory and ab initio Hartree–Fork studies on the structural parameters and chemical activity of the free radicals generated by benzoquinone and hydroquinone

Yuanzhi Song,[a,b] Jimin Xie,[a,*] Huoming Shu,[a] Ganqing Zhao,[a] Xiaomeng Lv[a] and Hongyan Cai[c]

[a]*School of Chemistry and Chemical Engineering, Jiangsu University, Zhenjiang 212013, PR China*
[b]*Chemistry Department, Huaiyin Teachers College, Huaian 223300, PR China*
[c]*Zhongnan Hospital, Wuhan University, Wu Han 4330070, PR China*

Received 14 March 2005; revised 16 May 2005; accepted 16 May 2005
Available online 1 July 2005

Abstract—Density-functional theory (DFT) calculations were performed for calculation of the theoretical spectra and chemical activities of free radicals generated by benzoquinone and hydroquinone as well as the transition states, and the calculated spectra were used for the assignment of the frequencies observed in the experimental IR spectra. The calculated geometrical parameters, the predicted IR spectra, and the chemical activities of free radicals and transition states were also compared with those of benzoquinone and hydroquinone. The reactive mechanisms of free radicals generated by benzoquinone and hydroquinone are also discussed using ab initio Hartree–Fork (HF) methods.

1. Introduction

Metabolites of benzene–catechol, hydroquinone (BQH_2), and particularly its oxidized form, benzoquinone (BQ), exert toxic effects on biomacromolecules, for example, by covalent binding to proteins, formation of DNA adducts,[1] and destruction of cytochrome P450 (CYP).[2–4] Benzene is an established human and animal carcinogen[5] acting through an epigenetic mechanism. BQ reacts efficiently with thiol groups and its reaction with highly nucleophilic thiols of tubulin is supposed to damage the mitotic spindle and mediate benzene myelotoxicity. It reacts spontaneously with DNA forming a DNA adduct[1] and indirectly damages DNA by the formation of reactive oxygen species, specifically hydrogen peroxide, which produces 8-hydroxydeoxyguanosine[6]. In air-saturated buffered aqueous solutions, BQH_2 undergoes slow auto-oxidation to produce the semiquinone radical ($BQH^{\cdot}$) and subsequently BQ.[7,8] During auto-oxidation of $BQH^{\cdot}$, superoxide anion radical is produced and may dismutate to H_2O_2.[9,10] H_2O_2 and the superoxide anion radicals form OH radicals in the Haber–Weiss reaction catalyzed by iron and BQ. OH radicals are especially very toxic for the cell as they damage DNA.[11] The microsomal membrane system is a complex of oxidative and reductive enzymes, among which CYP in conjunction with NADPH-dependent P450 reductase catalyzes oxidation of $BQH^{\cdot}$ to BQ, reduction of BQ to $BQH^{\cdot}$, and activity of oxygen.[12] Radicals or reactive oxygen species also originate during the futile CYP cycle.[13,14] The omnipresent iron activates oxygen even when bound to proteins and ascorbate also activates oxygen, especially in complex with iron,[15] which can damage CYP enzymes[3,4] and presumably other proteins. Interactions between BQ, iron, ascorbate, and the microsomal modify BQ toxicity. The outcome of their interactions may result in toxicity to the cell and promote diseases, for example, cancer.

The electrochemistry of BQH_2 has been studied widely in both aqueous and non-aqueous solutions.[16,17] The oxidation of BQH_2 to BQ follows the simple stoichiometry: $BQH_2 = BQ + 2H^+ + 2e^-$. Cyclic voltammetry, in situ UV–vis, and infrared spectroelectrochemistry have shown that hydroquinone anion (BQH^-) is

Keywords: DFT; HF; IR spectrum; Benzoquinone; Hydroquinone; Free radicals; Chemical activity.
* Corresponding author. Tel.: +86 511 5883326; fax: +86 511 8797786; e-mail: Xiejm391@sohu.com

0968-0896/$ - see front matter © 2005 Published by Elsevier Ltd.
doi:10.1016/j.bmc.2005.05.029

formed at negative potentials and this appears to arise via surface decomposition of BQH_2 to $BQH^{\bullet}$ followed by reaction of $BQH^{\bullet}$ with the *p*-benzoquinone radical anion ($BQ^{\bullet-}$). The oxidation of BQH^- appears to occur via disproportionation of $BQH^{\bullet}$ and leads to BQH_2 and BQ as the products, the free radicals are formed as shown below:[18]

$$BQH_2 = BQH^{\bullet} + H^{\bullet} \quad (1)$$

$$BQH^{\bullet} + BQ^{\bullet-} = BQ + BQH^- \quad (2)$$

$$BQ + e^- = BQ^{\bullet-} \quad (3)$$

Electron paramagnetic resonance (EPR) experiments showed that $BQH^{\bullet}$ and $BQ^{\bullet-}$ are observed in the presence of molecular oxygen as the mono-anion at pH 7 (buffered solution).[19] Under this condition, the free radical should also be present in the human body. Thus, it is very important to study the relationship between chemical properties and geometrical parameters of the free radicals.

Many study results have indicated that density-functional theory (DFT) is a powerful method for predicting the geometry and hormonic vibration of organic substances.[20–22] Therefore, DFT studies were carried out to study the molecular structure, the vibrational frequency, and properties of the free radicals generated by BQH_2 and BQ. The energy transfers of reaction were calculated using ab initio method.

The reactive mechanism from BQH_2 to BQ in solution is very complex; we select a reaction pathway without other compounds present in the reactants. The schemes of reaction pathways were shown in Figure 1 according to optimized structures of reactants, products, intermediates, and transition states (TS).

2. Calculation methods

Both DFT (UB3LYP)[23,24] and Hartree–Fork (UHF) methods,[25,26] using the 6-31G(d) basis set, were performed with Gaussian98W program[27] according to the multiplicities of electrons in the molecules. The total energies (E_t) and zero point energies (E_{ZPE}) of reactants, products, intermediates, and transition states were calculated at the UHF/6-31G(d) level. For transition states, intrinsic reaction coordinate (IRC) calculations were performed to determine the reactants of dissociation channels to which the transition state evolved. For comparison with ground states of BQH_2 and BQ, DFT (RB3LYP) methods at 6-31G(d) level were also performed.

The geometrical optimizations of the free radicals, BQH_2, BQ, intermediates, and transition states were performed under relaxation of all internal degrees of freedom. Note that the Opt = Tight and Int = FineGrid options of the free radicals, BQH_2, BQ, and intermediates whereas the infrared spectra were predicted at level with the Int = FineGrid option. The harmonic vibrational frequencies and infrared intensities were subsequently calculated by using the numerical differentiation of analytical gradients. The visualization of atom movement was made possible by using GaussView2.1.[28]

3. Results

3.1. Geometry

Humphrey and Pratt[29] have applied high resolution s_1–s_0 fluorescence excitation spectroscopy and nuclear spin statistical analysis to distinguish the cis and trans isomers of BQH_2. The ground state structures of the two isomers for BQH_2 were determined by microwave spectroscopy[30] and ab initio calculations.[31,32] Vibrational assignments have been done on the basis of

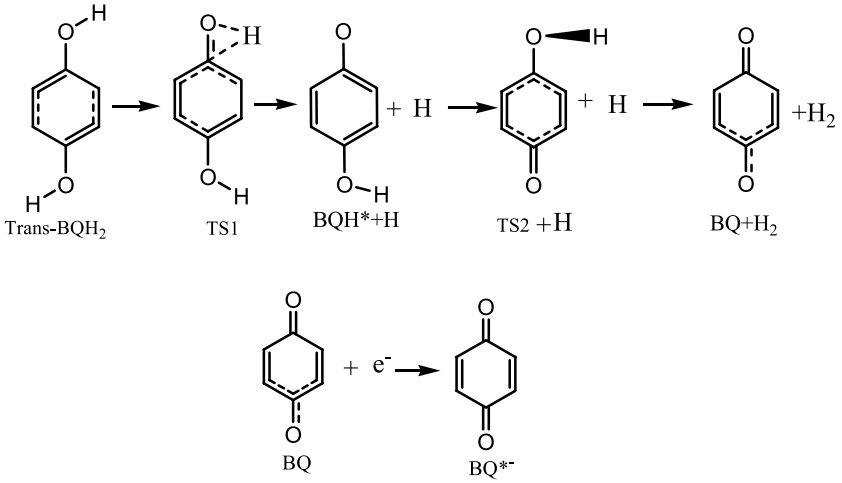

Figure 1. The schemes of reaction pathways.

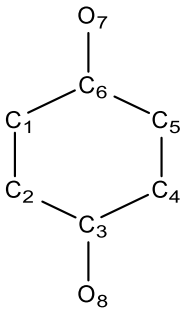

Figure 2. Numeration of BQH_2, BQ, TS, $BQH^{\cdot}$, and $BQ^{\cdot-}$.

liquid- and solid-phase infrared and Raman spectra.[33] The excited state structure and vibrations of BQH_2 and the vapor-phase infrared spectra of *trans*-BQH_2 have also been reported in the literature.[34,35]

In this paper, the calculated vibrational frequencies of *trans*-BQH_2, BQ, $BQH^{\cdot}$, and $BQ^{\cdot}$ using DFT methods at the UB3LYP/6-31G(d) level have no imaginary vibrational frequencies; however, an imaginary vibrational frequency at $-2498\ cm^{-1}$ of TS1 and another at $-262\ cm^{-1}$ of TS2 were found in the calculated spectrum. This indicates that the optimized geometries were reasonable and reliable. The numeration of atoms in *trans*-BQH_2, BQ, TS, and the free radicals are shown in Figure 2.

The bond lengths and bond angles for the excited states (*trans*-BQH_2 and BQ), TS1, TS2, $BQH^{\cdot}$, and $BQ^{\cdot-}$ optimized at the UB3LYP/6-31G(d) level as well as the ground states of *trans*-BQH_2 and BQ at the RB3LYP/6-31G(d) level are presented in Table 1. It can be seen from Table 1 that the bond lengths and angles calculated for *trans*-BQH_2 and BQ at RB3LYP/6-31G(d) level are in the good agreement with the values obtained in experiments.

The calculated bond lengths of C_2C_3, C_3C_4, C_5C_6, and C_1C_6 of $BQH^{\cdot}$ are longer than those of ground state of *trans*-BQH_2 at the RB3LYP/6-31G(d) level; however, the bond lengths of C_1C_2, C_4C_5, C_6O_7, and C_3O_8 of $BQH^{\cdot}$ are shorter than those of the ground state of *trans*-BQH_2 at the RB3LYP/6-31G(d) level. This can be explained by the fact that the oxygen atom that has lost a hydrogen strongly draws the electrons from other atoms in benzene ring. Furthermore, increase in the bond angles of $C_6C_1C_2$, $C_2C_3C_4$, and $C_4C_5O_6$ due to changes in the bond lengths are also observed. This reveals that the C_3O of $BQH^{\cdot}$ are tilted towards each other due to the intrinsic through-space attractive interaction between the oxygen atom and hydrogen atom attached to the corresponding ring carbon atoms.

With BQ getting an electron, the oxygen atom strongly draws the electron of other atoms in benzene ring, and thus the electron cloud shifts toward oxygen. The four calculated bond lengths, C_2C_3, C_3C_4, C_5C_6, and C_1C_6, of $BQ^{\cdot-}$ are shorter than those of BQ at the RB3LYP/6-31G(d) level, whereas the four calculated bong lengths, C_1C_2, C_4C_5, C_6O_7, and C_3O_8 of $BQ^{\cdot-}$ are longer. As a result, the bond angles of $C_6C_1C_2$, $C_1C_2C_3$, $C_3C_4C_5$, $C_4C_5C_6$, and $C_5C_6O_7$ in $BQ^{\cdot-}$ increase, whereas the bond angles of $C_2C_3C_4$ and $C_5C_6C_1$ in $BQ^{\cdot-}$ decrease, indicating that the interaction of C=O bond increases.

For a probe into structures of transition states (TS1 and TS2) optimized at the UB3LYP/6-31G(d) level, the bond angles and bond lengths of TS1 and TS2 are also summarized in Table 1. A comparison of these parameters shows that the bond angles and bond lengths of TS1

Table 1. The geometry parameter of *trans*-BQH_2, BQ, $BQH^{\cdot}$, and $BQ^{\cdot-}$

Method	*Trans*-BQH_2			TS1	$BQH^{\cdot}$	TS2	BQ			$BQ^{\cdot-}$
	Calcd		Exp.[36]	Calcd	Calcd	Calcd	Calcd		Exp.[37]	Calcd
	RB3LYP	UB3LYP		UB3LYP	UB3LYP	UB3LYP	RB3LYP	UB3LYP		UB3LYP
Bond length										
C_1C_2	1.390	1.420	1.390	1.351	1.372	1.385	1.343	1.371	1.344	1.372
C_2C_3	1.400	1.372	1.398	1.343	1.415	1.408	1.486	1.429	1.481	1.453
C_3C_4	1.395	1.488	1.392	1.450	1.413	1.408	1.486	1.429	1.481	1.453
C_4C_5	1.398	1.420	1.396	1.444	1.375	1.385	1.343	1.371	1.344	1.372
C_5C_6	1.395	1.372	1.392	1.428	1.453	1.440	1.486	1.453	1.481	1.453
C_1C_6	1.400	1.488	1.398	1.433	1.454	1.440	1.486	1.453	1.481	1.453
C_6O_7	1.373	1.354	1.377	1.264	1.256	1.253	1.225	1.254	1.225	1.266
C_3O_8	1.373	1.354	1.377	1.444	1.355	1.366	1.225	1.308	1.225	1.266
Bond angle										
$C_6C_1C_2$	120.3	117.4	120.0	117.5	121.6	120.4	121.4	122.4	121.0	122.7
$C_1C_2C_3$	120.3	119.8	120.0	119.1	119.8	120.1	121.4	119.1	121.0	122.7
$C_2C_3C_4$	119.5	122.7	120.0	120.7	120.8	120.8	117.3	120.8	118.1	114.6
$C_3C_4C_5$	120.2	117.4	120.0	123.4	120.0	120.1	121.4	119.1	121.0	122.7
$C_4C_5C_6$	120.0	119.8	120.0	115.8	121.4	120.4	121.4	122.4	121.0	122.7
$C_5C_6C_1$	119.5	122.7	120.0	121.8	116.4	118.2	117.3	116.0	118.1	114.6
$C_5C_6O_7$	123.1	124.2	123.0	128.4	121.7	120.9	121.4	122.0	121.0	122.7
$C_2C_3O_8$	123.1	119.8	123.0	109.0	122.3	119.6	121.4	119.6	121.0	122.7

Calcd and Exp. represent calculated values and experimental values, respectively.

have changed. It is specially noticed that the bond length of C_3O_8 in TS1 is longer than that of BQ, $BQH^{\cdot}$, *trans*-BQH_2, and $BQ^{\cdot-}$. The results indicate that the OH bond of TS1 is active group, which leads to the generation of BQ. However, compared with ground states of BQ and BQH_2, both the bond lengths and bond angles in TS2 and BQH_2 of excited states have very few changes. In addition, the bond length of C_3O_8 in BQ of excited states has changed markedly.

3.2. Vibration

The theoretical spectrum calculated using DFT method and experimental spectrum of *trans*-BQH_2 and BQ are shown in Figure 3. The ordinate is the IR relative intensity and the abscissa represents frequency (cm^{-1}). Figure 3 shows that general appearance of the calculated spectra of the ground states of BQ and BQH_2 at the RB3LYP/6-31G(d) level are in agreement with the experimental ones. The calculated frequencies and infrared intensities are listed in Table 2. The calculated frequencies are scaled by 0.96.[38]

The good overall agreement with experimental data for the ground states of *trans*-BQH_2 and BQ confirms the reliability of the band assignment presented. From the above results, it is concluded that the predicted infrared spectra for the $BQH^{\cdot}$ and $BQ^{\cdot-}$ investigated here should also be reliable. Due to the fact that there are deviations of the infrared intensities between the experimental data and the calculated spectra, some peaks could not be found in the experiment but can be observed in the calculated spectra. The peaks that can be found in both the calculated and the experimental spectra are important. Therefore, we simply discuss the peaks found in the experimental spectra and the stronger infrared intensities in the calculated spectra.

The strongest peak in the calculated spectrum of *trans*-BQH_2 at the RB3LYP/6-31D(d) level appears at 1164 cm^{-1}, which represents the in-plane bending of CH in benzene ring. The strongest experimental band is located at 1157 cm^{-1}, whereas the calculated strongest peak of $BQH^{\cdot}$ appears at 1573 cm^{-1}, which represents torsion of the benzene ring. Two modes, which are associated mainly with the OH stretching of *trans*-BQH_2 at the RB3LYP/6-31G(d) level, are assigned to the band located at 3607 cm^{-1} in the calculated spectrum, whereas its experimental frequency appeared at 3652 cm^{-1}. However, the band of the OH stretching in $BQH^{\cdot}$ was found at 3588 cm^{-1}. The bands of the CH stretching, CO stretching, and CC stretching of *trans*-BQH_2 at the RB3LYP/6-31G(d) level in calculated spectrum are located at 3037, 1236, and 736 cm^{-1}, whereas the experimental frequencies appear at 3026, 1257, and 742 cm^{-1}, respectively. Furthermore, the frequencies of predicted CH stretching, CO stretching, and CC stretching of $BQH^{\cdot}$ are located at 3037, 1468, and 1274 cm^{-1}, respectively. The frequencies of CC stretching of $BQH^{\cdot}$ are higher than that of *trans*-BQH_2 at the RB3LYP/6-

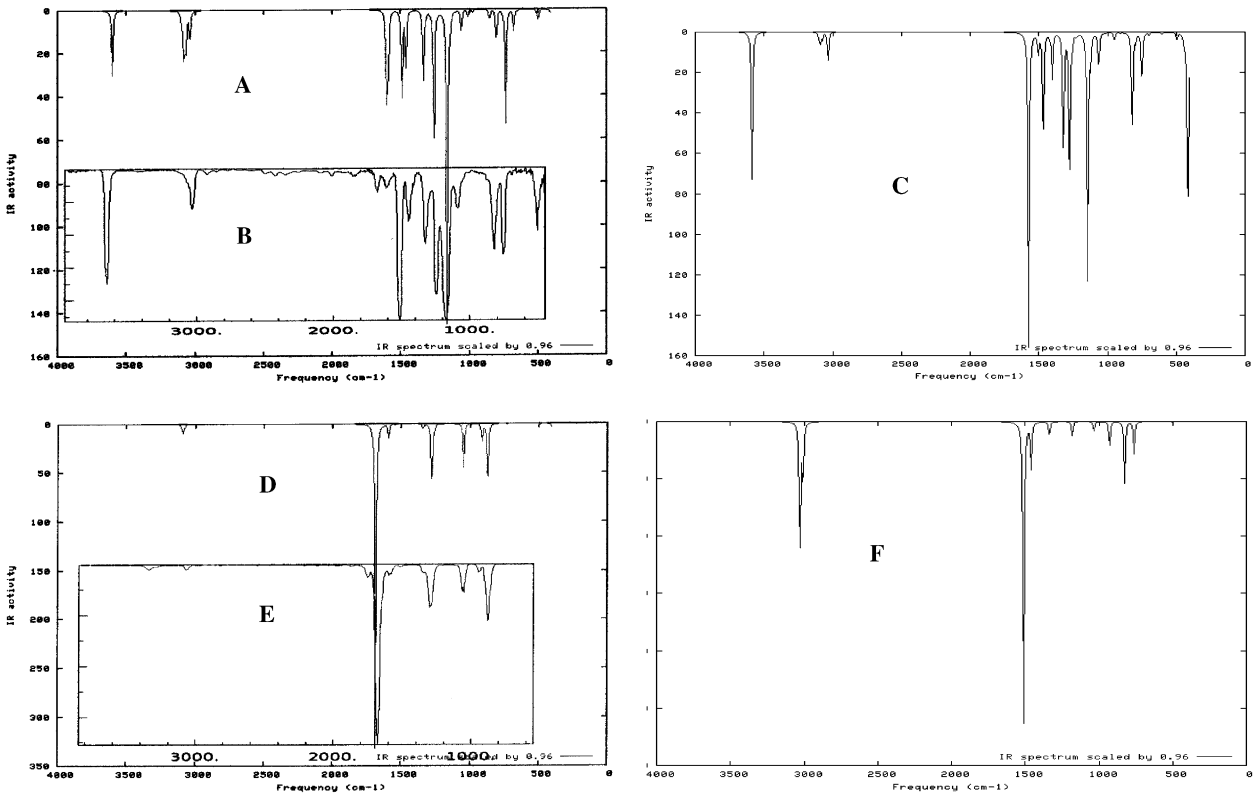

Figure 3. The theoretical frequencies and IR spectrum of BQ, BQH_2, $BQ^{\cdot-}$, and $BQH^{\cdot}$. No. A, No. C, No. D, and No. F represent the theoretical spectrum of *trans*-BQH_2 at RB3LYP/6-31G(d) level, $BQH^{\cdot}$ at UB3LYP/6-31G(d) level, BQ at RB3LYP/6-31G(d) level and $BQ^{\cdot-}$ at UB3LYP/6-31G(d), respectively. No. B and No. E represent experimental spectrum of *trans*-BQH_2 and BQ. The theoretical spectrum are scaled by 0.96[38].

Table 2. Experimental ($\nu_{Exp.}$) and calculated (ν_{Calcd}) vibrational wavenumber (cm^{-1}), IR absorption intensities (I, km/mol), Exp. represents experimental values

Trans-BQH_2 Exp.1 (cm^{-1})[39]	*Trans*-BQH_2 RB3LYP ν_{Calcd} (cm^{-1}) (I)	*Trans*-BQH_2 UB3LYP ν_{Calcd} (cm^{-1}) (I)	TS1 UB3LYP ν_{Calcd} (cm^{-1}) (I)	$BQH^{\cdot}$ UB3LYP ν_{Calcd} (cm^{-1}) (I)	TS2 UB3LYP ν_{Calcd} (cm^{-1}) (I)	BQ Exp. 2 (cm^{-1})[40]	BQ RB3LYP ν_{Calcd} (cm^{-1}) (I)	BQ UB3LYP ν_{Calcd} (cm^{-1}) (I)	Exp. 3 (cm^{-1})[18]	$BQ^{\cdot-}$ UB3LYP ν_{Calcd} (cm^{-1}) (I)
	3607(29.0)	3566(29.0)	−2398(742.5)	3588(73.9)	3912(106.9)		3094(0.00)	3101(2.9)		3036(0.00)
3652	3607(45.6)	3566(66.5)	3606(37.9)	3124(2.5)	3263(0.0)	3072	3092(9.0)	3100(0.2)		3031(130.1)
	3094(5.9)	3132(0.0)	3097(3.3)	3093(4.4)	3262(10.0)		3077(2.9)	3082(0.0)		3010(0.00)
	3081(5.6)	3133(0.0)	3075(3.6)	3080(3.9)	3245(8.0)		3076(0.1)	3081(0.1)		3010(32.4)
	3054(17.3)	3129(4.6)	3047(18.8)	3037(17.1)	3246(3.2)	1685	1688(332.8)	1490(51.0)		1606(0.00)
3026	3037(23.0)	3042(0.0)	2971(2.7)	1573(156)	1604(131.1)		1687(0.0)	1446(9.1)	1505	1510(299.1)
	1619(0.1)	1555(354.2)	1704(8.0)	1503(11.3)	1541(7.2)		1626(0.00)	1430(1.7)		1465(0.00)
1616	1599(13.0)	1528(0.0)	1596(7.8)	1468(64.2)	1511(0.3)	1592	1593(16.2)	1391(3.0)		1459(40.8)
1510	1514(212.7)	1407(49.66)	1509(30.4)	1419(2.5)	1455(0.1)		1350(0.00)	1342(0.0)		1403(0.00)
	1452(0.00)	1392(0.0)	1478(421.0)	1401(22.8)	1360(29.5)	1344	1340(5.4)	1237(40.8)	1344	1332(16.2)
	1329(9.3)	1355(17.2)	1404(29.0)	1318(73.3)	1336(13.7)	1260	1275(80.8)	1231(0.4)		1215(0.00)
1350	1318(112.9)	1295(0.0)	1346(41.5)	1274(91.4)	1324(3.2)		1191(0.00)	1178(6.1)		1183(13.2)
	1262(0.1)	1249(100.5)	1344(29.0)	1225(1.3)	1308(6.7)		1128(0.00)	1118(8.1)		1115(0.00)
1257	1236(130.0)	1220(0.0)	1237(23.3)	1147(123.2)	1266(239.3)	980	1046(48.7)	1062(8.2)		1035(9.4)
1157	1164(318.4)	1159(359.6)	1215(1.2)	1126(0.09)	1160(26.8)		987(0.00)	928(3.8)		927(24.8)
	1153(8.6)	1146.5(0.0)	1154(113.7)	1066(13.6)	1117(5.8)		976(0.00)	900(1.2)		912(0.00)
	1149(1.7)	1023(66.7)	1140(76.5)	950(21.4)	1014(1.0)		913(18.6)	894(0.0)		908(0.00)
	1079(10.4)	978(0.0)	1101(67.5)	932(0.00)	957(0.00)	887	871(75.1)	805(63.1)		824(53.7)
	988(0.00)	891(105.3)	1050(58.8)	906(0.00)	945(1.4)		766(0.00)	792(1.3)		790(0.00)
	909(0.00)	766(0.0)	954(10.3)	820(60.1)	837(78.0)		746(0.00)	741(0.0)		759(28.7)
	850(0.0)	752(0.0)	940(1.0)	795(3.8)	826(1.2)		732(0.00)	740(18.4)		749(0.00)
	834(0.00)	751(78.0)	842(6.3)	754(4.2)	793(0.2)		726(0.00)	641(9.1)		726(0.00)
813	807(39.0)	720(18.7)	817(20.1)	749(26.5)	788(13.5)		578(0.00)	588(0.3)		609(0.00)
	759(21.5)	584(0.0)	787(50.6)	696(1.6)	685(6.6)		495(1.68)	480(3.3)		503(1.3)
742	736(48.0)	560(0.0)	778(34.3)	607(1.2)	642(0.1)		437(0.00)	439(1.5)		450(0.00)
	674(0.00)	502(76.4)	724(18.4)	496(4.5)	502(11.0)		436(0.00)	432(0.1)		450(0.00)
	633(2.21)	492(0.0)	625(2.0)	447(0.8)	477(3.3)		396(25.6)	374(0.0)		381(0.00)
500	503(9.6)	476(125.8)	595(28.7)	442(5.2)	466(0.2)		325(0.00)	326(8.6)		375(0.00)
	452(0.3)	413(0.0)	501(6.5)	418(114.6)	386(0.5)		232(0.00)	304(0.4)		317(0.00)
471	430(22.6)	403(0.0)	468(16.0)	371(8.9)	378(10.1)		95(13.0)	127(6.4)		132(10.9)
	409(0.00)	333(17.8)	438(4.7)	354(10.3)	326(7.3)					
	355(0.00)	261(0.0)	387(3.4)	311(4.4)	142(4.9)					
	329(0.00)	257(0.48)	356(13.3)	131(2.4)	−262(138.1)					
	306(243.7)	171(0.15)	318(56.8)							
	300(0.00)	165(75.3)	310(69.5)							
	152(0.2)	59(3.6)	146(3.4)							

31G(d) level. This can be explained based on the fact that the C–O and C–C bonds become stronger due to the increased interaction between the ring and the oxygen atom when the oxygen has lost a hydrogen. This causes an increase in the corresponding force constant leading to an increase in frequency. Three predicted bands of in-plane bending of CH located at 1599, 1514, and 1236 cm^{-1} in ring of *trans*-BQH_2 at the RB3LYP/6-31G(d) level is observed in the experimental IR spectrum at 1510, 1350, and 1257 cm^{-1}, respectively. The predicted bands at 1274, 1147, 1126, and 1066 cm^{-1} are assigned to the CH in-plane bending of $BQH^{\cdot}$. In addition, the bands of the stronger benzene torsion of $BQH^{\cdot}$ were found at 1401, 1318, and 749 cm^{-1}.

The band observed at 3072 cm^{-1} in the IR spectrum of BQ is in good agreement with that of CH stretching located at 3092 cm^{-1} in the calculated spectrum at the RB3LYP/6-31G(d) level. The strongest peak due to C=O stretching of BQ located at 1685 cm^{-1} in the experiment appeared at 1688 cm^{-1} in the calculated spectrum at the RB3LYP/6-31G(d) level. The band located at 1510 cm^{-1} in the calculated spectrum of $BQ^{\cdot-}$ was found at 1505 cm^{-1} in the in situ IR spectrum.[18] This can be explained by the fact that the CO bond is weaker due to the decreased interaction between the ring and the oxygen atom as BQ accepts an electron. The peak located at 1344 cm^{-1} in the in situ IR spectrum[18] may be assigned to the CH in-plane bending in $BQ^{\cdot-}$, which is located at 1332 cm^{-1} in the calculated spectrum but is not found in BQ at the RB3LYP/6-31G(d) level. Two bands of benzene ring torsion found at 1593 and 1275 cm^{-1} in the calculated spectrum of BQ at the RB3LYP/6-31G(d) level are assigned to the frequencies located at 1592 and 1260 cm^{-1} in the the experimental spectrum, respectively. One band of in-plane bending located at 1340 cm^{-1} and another band of out-plane bending located at 871 cm^{-1} of BQ at the RB3LYP/6-31G(d) level in the calculated spectrum are observed at 1344 and 887 cm^{-1}, respectively, in the experimental spectrum. Two bands of the stronger benzene torsion in the calculated spectrum of $BQ^{\cdot-}$ located at 1459 and 759 cm^{-1} were assigned respectively, to the in-plane bending located at 1459 cm^{-1} and to the out-plane bending located at 759 cm^{-1}.Therefore, it is easy to assign the new peaks found in the in situ IR spectrum from the calculated spectrum.

An imaginary vibrational frequency at -2498 cm^{-1} in the calculated spectrum of TS1 represents H vibration, and the imaginary vibrational frequency at -262 cm^{-1} in the calculated spectrum of TS2 level represents the vibration of benzene torsion. This indicates that the structures of TS1 and TS2 are reliable.

A comparison with the frequencies of ground states, shows that the frequencies of excited states of BQ and *trans*-BQH_2 at the UB3LYP/6-31G(d) level in the region lower than 1600 cm^{-1} shift to the lower values; however, their relative intensities are stronger than those of ground states.

3.3. Distribution of Mülliken charges

Distribution of Mülliken charges of molecules are shown in Table 3. It is clear from Table 3 that the Mülliken charges of C_1, C_3, and C_4 in $BQH^{\cdot}$ are slightly positive than those of C_1, C_3, and C_4 in *trans*-BQH_2 at the RB3LYP/6-31G(d) level. However, the Mülliken charges of electron-withdrawing O_7 in $BQH^{\cdot}$ are markedly more negative than those of O_7 in *trans*-BQH_2, whereas Mülliken charges of O_8 and C_6 in $BQH^{\cdot}$ are more positive than those of O_8 and C_6 in *trans*-BQH_2 at the RB3LYP/6-31G(d) level. Thus, the hydrogen bonds form easily between the oxygen of $BQH^{\cdot}$ and that such as the adjacent amide groups of DNA bases, or the positive charges of C_6 in $BQH^{\cdot}$ strongly attract the phosphate groups of DNA bases. The Mülliken charges of electron-withdrawing O_7 and O_8 in $BQ^{\cdot-}$ are markedly more negative than those of O_7 and O_8 in BQ at the RB3LYP/6-31G(d) level. Therefore, the free radicals generated by BQ and *trans*-BQH_2 are more active than *trans*-BQH_2 and BQ of ground stases. Because O_7 loses hydrogen, the Mülliken charges of C_6 in TS1 and O_8 in TS1 as well as in TS2 have changed markedly. However, compared with the Mülliken charges of ground states of BQ and BQH_2 at the B3LYP/6-31G(d) level, except O_8 and C_3 of BQ at the UB3LYP/6-31G(d) level, the Mülliken charges of BQH_2 and BQ at UB3LYP/6-31G(d) level have few changes.

3.4. The eigenvalues of LUMO and HOMO

The eigenvalues of LUMO and HOMO and its energies gap reflect the molecular activity. LUMO as an electron acceptor represents the ability to obtain electrons, and HOMO as an electron donor represents the ability to donate electrons. The lesser the energy gap between

Table 3. Distribution of Mülliken charges for *trans*-BQH_2, BQ, TS, $BQH^{\cdot}$, and $BQ^{\cdot}$

Method	*Trans*-BQH_2		TS1	$BQH^{\cdot}$	TS2	BQ		$BQ^{\cdot-}$
	B3LYP	UB3LYP	UB3LYP	UB3LYP	UB3LYP	B3LYP	UB3LYP	UB3LYP
C_1	−0.021503	−0.096085	−0.041263	−0.018282	−0.000340	0.010212	−0.006758	−0.130377
C_2	−0.021503	−0.078712	0.078295	0.009012	0.002718	0.010213	0.002208	−0.130377
C_3	0.346627	0.351764	0.359546	0.352470	0.353697	0.434316	0.376797	0.394852
C_4	−0.080010	−0.096085	−0.023801	−0.047309	0.002713	0.010213	0.002208	−0.130377
C_5	−0.080010	−0.064443	−0.374961	−0.016570	−0.000334	0.010212	−0.006758	−0.130377
C_6	0.346627	0.351764	0.592728	0.411285	0.420994	0.434316	0.417944	0.394852
O_7	−0.245114	−0.191235	−0.282786	−0.497799	−0.470794	−0.454741	−0.497159	−0.634098
O_8	−0.245114	−0.191235	−0.307757	−0.192898	−0.308654	−0.454741	−0.288480	−0.634098

the LUMO and the HOMO, the easier it is for electrons of HOMO to be excited. The highest occupancy eigenvalue (HOMO) and the lowest virtual eigenvalue (LUMO) calculated using the DFT method are shown in Table 4 and Figure 4. The results in Table 3 and Figure 4 show that the energy gap of the front orbit energy of $BQH^{\cdot}$ is less than that of *trans*-BQH_2 at the RB3LYP/6-31G(d) level, and the energy gap of beta electrons in $BQ^{\cdot}$ is less than that of BQ at the RB3LYP/6-31G(d) level, indicating that the electrons of $BQ^{\cdot-}$ and $BQH^{\cdot}$ are easily excited. The energies of HOMO in $BQ^{\cdot-}$ increase, whereas the energies of LUMO in $BQ^{\cdot-}$ decrease. As a result, the free radicals generated by BQH_2 and BQ are more active than *trans*-BQH_2 and BQ at the RB3LYP/6-31G(d) level. In addition, compared with the energies of HOMO and LUMO, the energies of HOMO of *trans*-BQH_2 at the RB3LYP/6-31G(d) level is higher than that of BQ and the energies of LUMO of BQ at the RB3LYP/6-31G(d) level is lower than that of *trans*-BQH_2. In other words, BQ is an acceptor of electrons, and *trans*-BQH_2 is a donor of electrons. With the energies of the LUMO decreasing, TS1 could accept electrons, however, with the energies of the HOMO increasing, TS2 could donate electrons. Both the energies of LUMO of beta electrons and energy gap between LUMO and HOMO in BQH_2 at the UB3LYP/6-31G(d) level are less than those of BQH_2 at the RB3LYP/6-31G(d) level, and energies of HOMO of alpha electrons in BQH_2 at the UB3LYP/6-31G(d) level are higher than that of BQH_2 at the RB3LYP/6-31G(d) level. The energies of HOMO of beta electrons in BQ at the UB3LYP/6-31G(d) level are higher than that of BQ at the RB3LYP/6-31G(d), and the energy gap between HOMO and LUMO of beta electrons are less than that of BQ at the RB3LYP/6-31G(d) level. These results show that BQ and BQH_2 at the UB3LYP/6-31G(d) are active.

3.5. The mechanism of free radicals generated

As is known, the excited states of BQ and BQH_2 at the UB3LYP/6-31G(d) level, which has two electrons spining in the same direction, are active molecules in the reactions. The free radicals (intermediates), transition states (TS1 and TS2), BQ, and *trans*-BQH_2 of excited states were optimized at the UHF/6-31G(d) level. The total energies ($E_t = \varepsilon_0 + E_{ZPE}$) of reactants, products, intermediates, and transition states calculated at the same level are summarized in Table 5. ε_0 and E_{ZPE} represent electrons energies and zero point energies of the molecule, respectively.

Figure 5 shows the energy transfer from excited states to products and the activation energies of the reaction. It can be observed that *trans*-BQH_2 absorbs 127.14 kJ/mol from excited state to TS1. The reaction occurs easily in such a system in the presence of oxygen and BQH_2 because oxidation reaction of BQH_2 accompanied by the reduction of O_2 to H_2O will provide energies as below

$$\Delta G = -nF(E^0_{O_2/H_2O} - E^0_{BQ/BQH_2}) = 2 \times 96.5 \times (1.229 - 0.699) = 102.29\ \text{kJ/mol}$$

or

$$\Delta G = -nF(E^0_{O_2/H2O_2} - E^0_{BQ/BQH_2}) = 2 \times 96.5 \times (1.770 - 0.699) = 206.70\ \text{kJ/mol},$$

where ΔG is the standard transformed Gibbs energy of reaction, E^0_{O2/H_2}, $E^0_{BQ/BQH}$, and $E^0_{O_2/H_2O_2}$[41] represent the standard electrode potentials, respectively, n is the number of electrons transferred, and F is Faraday's constant. If sunlight with wavelength from 200 to 750 nm, which provide energies from 598 to 164 kJ/mol, or other compounds such as NADH and NADPH are present in the

Table 4. The eigenvalues of LUMO and HOMO

Molecule	E_{LUMO} (eV)	E_{HOMO} (eV)	$E_{LUMO}-E_{HOMO}$ (eV)
Trans-BQH_2(B3LYP)	−0.05878	−5.41892	5.36014
Trans-BQH_2(U3LYP)			
Alpha electrons	0.61444	−2.2327	2.84714
Beta electrons	−3.17913	−6.22220	3.04307
$BQH^{\cdot}$(UB3LYP)			
Alpha electrons	−0.62641	−5.59008	4.96367
Beta electrons	−3.22485	−6.44752	3.22227
BQ(B3LYP)	−3.53726	−7.36319	3.82595
BQ(UB3LYP)			
Alpha electrons	−0.94751	−5.78954	4.84203
Beta electrons	−3.17913	−6.65432	3.47519
$BQ^{\cdot-}$(UB3LYP)			
Alpha electrons	4.48175	0.36110	4.12065
Beta electrons	2.42619	−1.35242	3.77861
TS1(UB3LYP)			
Alpha electrons	−1.74807	−5.44232	3.69425
Beta electrons	−1.74807	−5.44232	3.69425
TS2(UB3LYP)			
Alpha electrons	0.61444	−2.23271	2.84715
Beta electrons	3.84799	−9.51099	5.66300

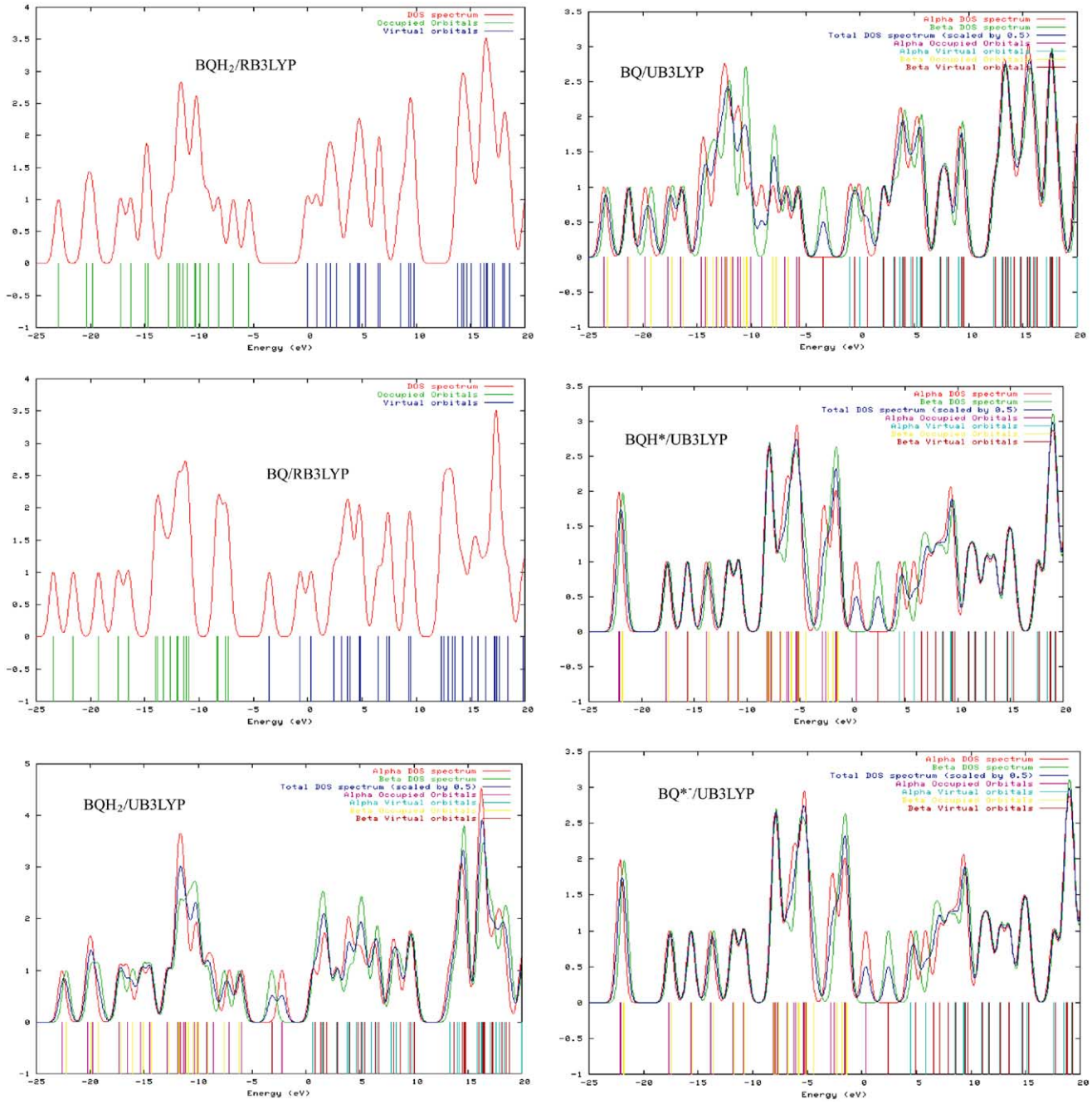

Figure 4. Occupied molecular orbital and unoccupied molecular orbital of *trans*-BQH_2, BQ, BQH$^{\cdot}$, and $BQ^{\cdot -}$.

Table 5. The energies of reactants, products, intermediates, and transition states

	ε_0 (Hartree)	E_{ZPE} (Hartree)	E_t (Hartree)
Trans-BQH_2	−380.314891	0.109386	−380.205505
BQH$^{\cdot}$	−379.829319	0.100935	−379.728384
TS1	−380.2671131	0.110032	−380.1570811
TS2	−379.8254123	0.099849	−379.7255633
$BQ^{\cdot -}$	−379.2624595	0.089772	−379.1726875
BQ	−379.2082518	0.087470	−379.1207818
H	−0.4982329	0.0000000	−0.4982329
BQ + H_2	−380.3351901	0.098570	−380.2366201

solution (its standard electrode potential is lower than that of BQH_2), the free radicals generated more easily.

From the results of LUMO of BQ in Table 4, BQ obtains an electron easily. BQH$^{\cdot}$ and $BQ^{\cdot -}$ located at higher energies level are unstable, which have a tendency of bonding with other compounds such as DNA and protein as the energy of the process decreases.

The activation energy in going from BQH$^{\cdot}$ to TS2 is 7.41 kJ/mol, which could be provided easily by the oxidation reaction of BQH_2.

For validation of TS1 and TS2 IRC,[42–44] calculations were performed to determine the reactant or product channels to which the transition states evolved. Figure 6 shows that the path could be followed in both directions from the point of TS1. The changes of

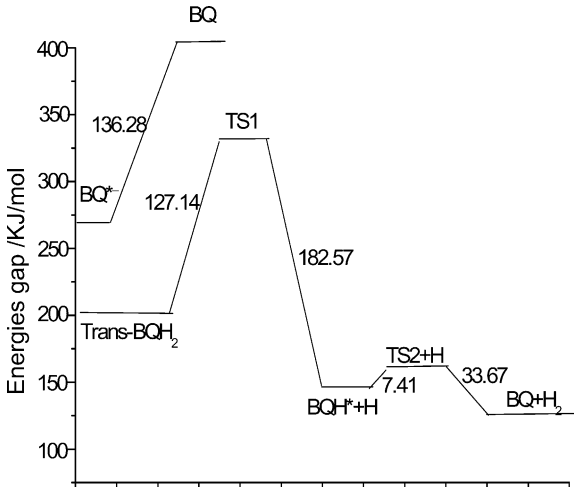

Figure 5. The energies transfer from reactant to product and the activation energies of reaction.

molecular energies and geometry are in agreement with that of TS1 and TS2 calculation. Figure 7 shows changes of the energies with molecular geometry in a process that goes from reactants to products. These results indicate that the TS1 calculation is reliable.

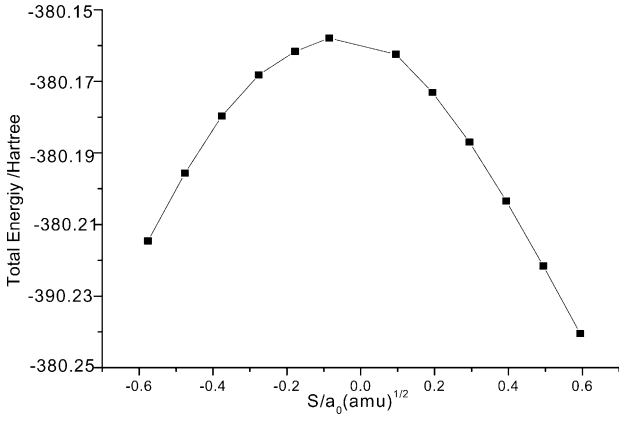

Figure 6. RIC reaction coordinate of TS, s represents the molecular geometry.

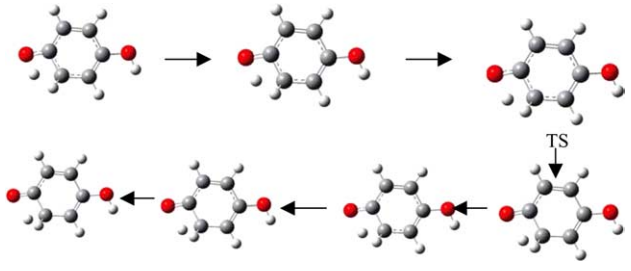

Figure 7. The changes of molecular geometry in a process from reactant to product.

4. Conclusion

The molecular property of a compound is controlled by its molecular geometry. The IR vibrational frequencies of *trans*-BQH_2, BQ, TS, $BQ^{\cdot -}$, and $BQH^{\cdot}$ were predicted using the DFT method. The calculated spectra of *trans*-BQH_2 and BQ at the B3LYP/6-31G(d) level are in agreement with the experimental ones. Hence the geometries of *trans*-BQH_2, BQ, $BQ^{\cdot -}$, TS, and $BQH^{\cdot}$ can be considered as reliable. The calculation of TS indicated that free radicals are generated easily in aqueous solution and in human body in which oxygen and BQH_2 are present if the deoxidized states such as NADH, NADPH, and ascorbic acid exist in it. Mülliken charges, TS calculation, and the front orbit energies of *trans*-BQH_2, BQ, $BQH^{\cdot}$, and $BQ^{\cdot -}$ indicate that $BQH^{\cdot}$ and $BQ^{\cdot -}$, which are generated easily by BQH_2 and BQ, are more active, and are harmful to the human body.

Acknowledgments

This research was supported by the National Youth Sciences Foundation of China (Grant No. 20302002) and by the Science Foundation of Education department of Jiangsu province of China (Grant No. 04KJD150038).

References and notes

1. Ross, D. *Eur. J. Hematol* **1996**, *57* (Suppl.), 111.
2. Nelson, D. R.; Koymans, L.; Kamataki, T.; Stegeman, J. J.; Feyereisen, R.; Waxman, D. J.; Waterman, M. R.; Gotoh, O.; Coon, M. J.; Estabrook, R. W.; Gunsalus, I. C.; Nebert, D. W. *Pharmacogenetics* **1996**, *6*, 1.
3. Soucek, P.; Filipcova, B.; Gut, I. *Biochem. Pharmacol.* **1994**, *47*, 2233.
4. Soucek, P. *Chem. Biol. Interact.* **1999**, *121*, 223.
5. *IARC Monographs on the Evaluation of Carcinogenic Risk to Humans*. An Updating of IARC Monographs, Vols. 1–42, Suppl. 7, Lyon, France, 1987.
6. Leanderson, P.; Tagesson, C. *Chem. Biol. Interact.* **1990**, *75*, 71.
7. Zang, L. Y.; Stone, K.; Pryor, W. A. *Free Radical Biol. Med.* **1995**, *19*, 161.
8. Li, Y.; Kuppusamy, P.; Zweier, J. L. *Mol. Pharmacol.* **1996**, *49*, 404.
9. Tayama, S.; Nakagawa, Y. *Mutat. Res.* **1994**, *324*, 121.
10. Miura, Y. H.; Tomita, I.; Hirayama, T.; Fukui, S. *Biol. Pharm. Bull.* **1998**, *21*, 93–96.
11. Aruoma, O. I.; Halliwell, B.; Dizdaroglu, M. *J. Biol. Chem.* **1989**, *264*, 13024.
12. Tichavska, B.; Gut, I. *Chemicke Listy* **1994**, *88*, 580.
13. Schaefer, T. M.; Harris, F. P.; Guengerich, F. P. *Biochemistry* **1985**, *24*, 3254.
14. Guengerich, F. P.; Strickland, T. W. *Mol. Pharmacol.* **1977**, *13*, 993–1004.
15. Sies, H.; Cadenas, E. In *Biological Basis of Detoxication*; Caldwell, J., Jakoby, W. B., Eds.; Academic Press: New York, 1983, p 181.
16. Chambers, J. Q. In *The Chemistry of the Quinonoid Compounds*; Patai, S., Ed.; Wiley: New York, 1974, Chapter 14.

17. Chambers, J. Q. In *The Chemistry of the Quinonoid Compounds*; Patai, S., Rappoport, Z., Eds.; Wiley: New York, 1988; Vol. 2, Chapter 12.
18. Ali; Babaei; James, A. *McQuillan. J. Electroanal. Chem.* **1999**, *462*, 266.
19. Pedersen, J. A. *Spectrochim. Acta Part A* **2002**, *58*, 1257.
20. Scott, A. P.; Radom, L. *J. Phys. Chem.* **1996**, *100*, 16505.
21. Denis, P.; Ventura, O. N. *J. Mol. Struct.* **2001**, *537*, 173.
22. Bruynal, C.; Chandra, A. K.; Uchimaru, T.; Zeegers-Huyskens, Th. *Spectrochim. Acta Part A* **2000**, *56*, 591.
23. Lee, C.; Yank, W.; Parr, R. G. *Phys. Rev.* **1988**, *378*, 785.
24. Becke, A. D. *Chem. Phys.* **1993**, *98*, 5648.
25. Foresman, J. B.; Frish, A. E *Exploring Chemistry with Electronic Structure Methods*; Gaussian, Inc.: Pittsburgh, PA, 1996.
26. Jensen, F. *Introduction to Computational Chemistry*; Wiley: Chichester, 1999.
27. Frisch, M. J.; Trucks, G. W.; Schlegel, H. B.; Scuseria, G. E.; Robb, M. A.; Cheeseman, J. R.; Zakrzewski, V. G.; Montgomery, J. A., Jr.; Stratmann, R. E.; Burant, J. C.; Dapprich, S.; Millam, J. M.; Daniels, A. D.; Kudin, K. N.; Strain, M. C.; Farkas, O.; Tomasi, J.; Barone, V.; Cossi, M.; Cammi, R.; Mennucci, B.; Pomelli, C.; Adamo, C.; Clifford, S.; Ochterski, J.; Petersson, G. A.; Ayala, P. Y.; Cui, Q.; Morokuma, K.; Malick, D. K.; Rabuck, A. D.; Raghavachari, K.; Foresman, J. B.; Cioslowski, J.; Ortiz, J. V.; Baboul A. G.; Stefanov, B. B.; Liu, G.; Liashenko, A.; Piskorz, P.; Komaromi, I.; Gomperts, R.; Martin, R. L.; Fox, D. J.; Keith, T.; Al-Laham, M. A.; Peng, C. Y.; Nanayakkara, A.; Challacombe, M.; Gill, P. M. W.; Johnson, B.; Chen, W.; Wong, M. W.; Andres, J. L.; Gonzalez, C.; Head-Gordon, M.; Replogle, E. S.; Pople J. A., Gaussian 98 Gaussian, Inc.: Pittsburgh, PA, 1998.
28. GaussView 2.1 Gaussian, Inc, Garnegie office Park Pittsburgh, PA 15106, USA.
29. Humphrey, S. J.; Pratt, D. W. *J. Chem. Phys.* **1993**, *99*, 5078.
30. Caminati, W.; Melandri, S.; Favero, L. B. *J. Chem. Phys.* **1994**, *100*, 8569.
31. Kim, K.; Jordan, K. D. *Chem. Phys. Lett.* **1995**, *241*, 39.
32. Puebla, C.; Ha, T. *J. Mol. Struct. (Theochem.)* **1990**, *204*, 337.
33. Varsanyi, G. *Assignments of Vibrational Spectra of Seven Hundred Benzene Derivatives*; Wiley: New York, 1974.
34. Wilson, H. W. *Spectrochim. Acta Part A* **1974**, *30*, 2141.
35. Tzeng, W. B.; Narayanan, K.; Hsieh, C. Y. *Spectrochim. Acta Part A* **1997**, *53*, 2595.
36. Caminati, W.; Melandri, S.; Favero, L. B. *J. Chem. Phys.* **1994**, *100*, 8569.
37. Hagen, K.; Hedbery, K. *J. Chem. Phys.* **1973**, *59*, 158.
38. Scott, A. P.; Radom, L. *J. Phys. Chem.* **1996**, *100*, 16502.
39. Sabbah, R.; Buluku, E. N. L. E. *Can. J. Chem.* **1991**, *69*, 481.
40. Vassermann, A. *J. Chem. Soc.* **1935**, *3*, 828.
41. Dobos, D. *Electrochemical Data*, 1975.
42. Fukui, K. *J. Phys. Chem.* **1970**, *74*, 4161.
43. Gonzalez, C.; Schlegel, H. B. *J. Phys. Chem.* **1989**, *90*, 2154.
44. Gonzalez, C.; Schlege, H. B. I. *J. Phys. Chem.* **1979**, *70*, 1593.